

Detection loss tolerant supersensitive phase measurement with an SU(1,1) interferometer

Mathieu Manceau¹, Gerd Leuchs^{1,2}, Farid Khalili³ and Maria Chekhova^{1,2,3}

¹Max-Planck-Institute for the Science of Light, Erlangen, Germany

²University of Erlangen-Nürnberg, Staudtstrasse 7/B2, 91058 Erlangen, Germany

³Faculty of Physics, M V Lomonosov Moscow State University, Moscow, Russia

(Dated: May 14, 2022)

In an unseeded SU(1,1) interferometer composed of two cascaded degenerate parametric amplifiers, with direct detection at the output, we demonstrate a phase sensitivity overcoming the shot noise limit by 2.3 dB. The interferometer is strongly unbalanced, with the parametric gain of the second amplifier exceeding the gain of the first one by a factor of 2, which makes the scheme extremely tolerant to detection losses. We show that by increasing the gain of the second amplifier, the phase supersensitivity of the interferometer can be preserved even with detection losses as high as 80%. This finding can considerably improve the state-of-the-art interferometry, enable sub-shot-noise phase sensitivity in spectral ranges with inefficient detection, and allow extension to quantum imaging.

The sensitivity of an interferometric measurement on a phase shift depends on the state of light used as a probe and the measurement scheme. A measurement beating the precision given by a coherent state fed into a Mach-Zender interferometer, the so-called shot noise limit (SNL), is said to be supersensitive. In order to make super-sensitive phase measurements, quantum resources can be used. First proposed [1] and experimentally tested [2, 3] in the 1980-s, squeezed light is now used for gravitational wave detection [4, 5] beyond the shot noise limit. Supersensitivity can also be achieved with other quantum states [6, 7], which, however, are difficult to produce.

Besides the input state and the detection scheme, the structure of the interferometer can also be changed. Yurke et al. [8] proposed to use cascaded optical parametric amplifiers (OPAs) instead of the passive beam-splitters of conventional interferometric setups, the phase sensitive response of the OPAs giving rise to interference patterns. Such interferometers, usually called SU(1,1) interferometers, can display phase super-sensitivity without seeding the amplifiers [8]. Seeding can be used in order to increase the number of sensing photons and therefore the overall sensitivity [9]. It was recently theoretically noted that such a scheme involving two amplifiers can help overcoming the deleterious effects of optical losses [10, 11] on phase sensitivity. Note that losses occurring inside the interferometer have a different impact on the phase sensitivity

compared to losses due to elements external to the interferometer. These two kind of losses are therefore distinguished in the following and respectively called internal and external/detection losses. The influence of the latter kind of losses can be suppressed by the second amplifier. Indeed, amplifying the signal with the second OPA at the output of the interferometer while keeping the probing field constant eventually eliminates the effect of detection losses [12, 13].

Optical SU(1,1) interferometers have been implemented using two cascaded four-wave mixers [14, 15]. Recent experiments with this interferometer operated in the continuous-wave regime with seeding have demonstrated phase super-sensitivity [16] using homodyne detection. A truncated version, *i.e.* without a second amplifier, of the same scheme [17] has also demonstrated the possibility of supersensitive phase measurement. Finally, an atom SU(1,1) interferometer has shown sensitivity beyond the SNL [18] as well.

In this letter we report phase supersensitivity in an SU(1,1) interferometer formed by two cascaded nonlinear $\chi^{(2)}$ crystals. Our goal is to overcome the negative effect of detection losses by pumping the second OPA stronger than the first one. In the previous realizations of the SU(1,1) interferometer, both OPAs had the same absolute values of the parametric gain. However as shown theoretically in Ref. [13], the gain unbalancing leads to an increased tolerance of the setup to the detection losses. The

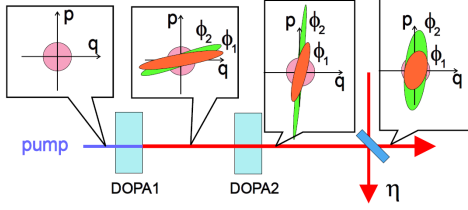


FIG. 1. Unbalanced unseeded SU(1,1) interferometer formed by coherently pumped DOPA1 and DOPA2. Squeezed vacuums with phases $\phi_{1,2}$ are distinguishable if their Wigner functions do not fully overlap. The squeezing after DOPA2 depends on the phase $\phi_{1,2}$ but the distinguishability remains the same. A low detection efficiency η almost destroys the squeezing but, with the DOPA2 gain high enough, the states remain distinguishable.

idea is illustrated in Fig. 1.

The interferometer consists of two degenerate parametric amplifiers, DOPA1 and DOPA2, the first one transforming an input vacuum state into a squeezed vacuum state, which then acquires a phase ϕ to be measured. Two squeezed vacuum states differing by their phases ϕ_1 and $\phi_2 = \phi_1 + \Delta\phi$ can be distinguished whenever their Wigner functions (shown by orange and green colors) do not completely overlap. Such squeezed vacuums have a higher distinguishability than two coherent states with the same photon number and the same phase difference $\Delta\phi$. The second amplifier DOPA2 applies squeezing opposite to the one of DOPA1, and the resulting output states are now squeezed in other directions, and differently as long as $\phi_1 \neq \phi_2$. Importantly, the squeezing operation does not change their distinguishability. In the presence of low detection efficiency η , represented in Fig. 1 by a beamsplitter, the states change dramatically, so that the noise in the squeezed quadrature becomes almost equal to the shot noise. At the same time, the spread of the anti-squeezed quadrature is only reduced by a factor $\sqrt{\eta}$, and will remain different for the two states as long as it is initially large. Therefore, provided that the DOPA2 gain is high enough, and the states at its output are highly squeezed, they are still distinguishable after the losses are applied. Note that the smaller the detection efficiency η , the stronger squeezing in DOPA2 is required to reach a certain phase sensitivity [13].

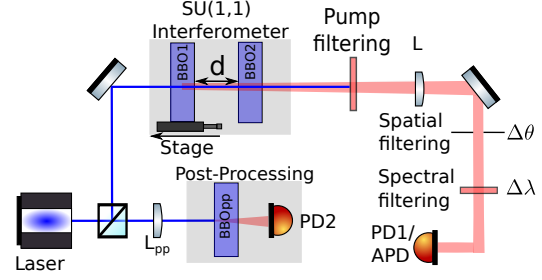


FIG. 2. The unseeded SU(1,1) interferometer is made of two cascaded BBO crystals, BBO1 and BBO2. The generated PDC light is spatially filtered by a pinhole placed in the focal plane of the lens L and spectrally filtered by an interference filter. The number of photons contained in a given PDC pulse is measured by the photodiode PD1. A second photodiode PD2 is used for post-selecting a pump intensity interval. An APD registers the number of photons emitted by BBO1 within the $\Delta\lambda$, $\Delta\theta$ bandwidths.

Although the same principle of unbalancing can be applied to various configurations of an SU(1,1) interferometer (seeded or unseeded, with direct or homodyne detection) and even to an SU(2) interferometer fed with squeezed light and followed by another squeezer [13], here we use the simplest configuration of an unseeded interferometer with direct intensity detection. The robustness of the measured phase sensitivity against detection losses is tested for various parametric gains of the DOPAs. We achieve a high parametric gain by using intense picosecond pump pulses and show the possibility to overcome the detrimental effect of losses for large parametric gain of the second DOPA.

The setup is depicted in Fig. 2. The SU(1,1) interferometer consists of two cascaded 3 mm long β -Barium Borate (BBO) crystals cut for collinear frequency-degenerate type-I phase matching. The pump is the second harmonic of a Spectra Physics Spitfire Ace system with a 5 kHz repetition rate, 1.5 ps pulses and a central wavelength of $\lambda_p = 400$ nm. The beam diameter is set to 0.2 mm full width at half maximum (FWHM) inside the SU(1,1) interferometer. Two dichroic mirrors are subsequently used to eliminate the pump beam. The parametric down converted (PDC) light generated by the SU(1,1) interferometer is spatially filtered by a pinhole in the focal plane of a $f = 90$ cm focal length

lens selecting an angular bandwidth $\Delta\theta$. An interference filter further selects a spectral bandwidth $\Delta\lambda$ around the central wavelength $\lambda_s = 800$ nm. After the spatial and spectral filtering, the PDC light is detected using a low-noise charge integrating p-i-n diode (PD)[19–21] (see supplementary).

The first crystal BBO1 is fixed on a translation stage. The distance d between the two crystals can therefore be changed. Due to the dispersion of the air [22], the squeezed light and the pump acquire different phase shifts $\phi_s \neq \phi_p$ in the air gap, and the phase $\phi = \phi_s - \phi_p/2$ of the squeezed state at the input of DOPA2 (Fig. 2) can be scanned by adjusting the distance d . A set of 4000 post-processed pulses is measured for each position of BBO1. To avoid high uncertainty in the determination of the measured mean photon number of the interferometer output light, the pump intensity fluctuations are eliminated through post-processing (see supplementary).

By measuring the transmission of the setup at $\lambda_s = 800$ nm, we found that the internal losses, caused by reflections on a single facet of each BBO crystal, are 3%. The external transmission of the setup, including the detector quantum efficiency, is measured to be $\eta = 77\%$. It corresponds to the losses for a set of plane waves within the $\Delta\lambda$, $\Delta\theta$ bandwidths of the frequency and spatial filters. The phase sensitivity $\Delta\phi$ is given by

$$\Delta\phi = \frac{\Delta N}{\left| \frac{\partial \langle N_f \rangle}{\partial \phi} \right|}, \quad (1)$$

ΔN being the photon noise, including the intrinsic photon noise of the measured light and the detector noise, and $\langle N_f \rangle$ the mean number of photons of the output interferometer state. For a given position d of BBO1, both values are determined from the set of post-processed pulses. The phase sensitivity is then calculated according to Eq. 1.

The distance between the two crystals is converted into a phase knowing the periodicity of the interference (see supplementary). Figure 3 presents typical phase sensitivity measurements. The shot noise limited phase sensitivity for a set of plane waves within the $\Delta\lambda$, $\Delta\theta$ bandwidths, $\Delta\phi_{SNL}$, is de-

finied as

$$\Delta\phi_{SNL} = \frac{1}{2\sqrt{\langle N(\Delta\lambda, \Delta\theta) \rangle}}, \quad (2)$$

with $\langle N(\Delta\lambda, \Delta\theta) \rangle$ being the mean number of photons inside the interferometer within the $\Delta\lambda$, $\Delta\theta$ bandwidths [13]. It is measured by removing BBO2 and registering the number of photons within the $\Delta\lambda$, $\Delta\theta$ bandwidths with an avalanche photodiode (APD) after attenuation of the beam with neutral density filters. The measured number of photons is rescaled to take into account the detection efficiency ($\eta_{APD} = 47\%$). The number of photons per Schmidt mode produced by the first crystal is $N_{mode} = \sinh(r_1)^2$. As we collect less than a single spatial Schmidt mode of the multimode PDC light, the resulting number of photons $\langle N(\Delta\lambda, \Delta\theta) \rangle$ is smaller than N_{mode} . For a single Schmidt mode of the multimode OPA, this narrowband detection is equivalent to losses [21, 23, 24], which leads to a detection efficiency $\eta_{SM} = v\eta$ much lower than η defined for plane waves. Here, v corresponds to the transmission of the spatial and frequency filters for the Schmidt mode under consideration. The SNL phase sensitivity associated to a single Schmidt mode, $\Delta\phi_{SM} = \frac{1}{2\sinh(r_1)}$, can still be beaten in theory with our large values of $|r_2|$ [12, 13]. However, the non ideal visibility, here being $\mathcal{V} = 97\%$ for the given spatial and frequency filtering (see supplementary), is a limiting factor for the best phase sensitivity achievable. Indeed, as the working point of this interferometer is close to the dark fringe, the non-unity visibility acts as an extra source of noise that is non negligible at the working point. $\Delta\phi_{SM}$ can therefore not be reached with the current experimental configuration.

Fig. 3a shows two measurements with different parametric gain values r_1 of the first crystal, and therefore different mean numbers of photons $\langle N(\Delta\lambda, \Delta\theta) \rangle$, varied by changing the phase matching. The blue curve corresponds to $\langle N(\Delta\lambda, \Delta\theta) \rangle = 1.7$ photons and $r_1 = 1.5$. The corresponding shot noise limited phase sensitivity is marked by the dashed blue line, $\Delta\phi_{SNL} = 0.38$ rad, the uncertainty is shown by the blue rectangle. The best phase sensitivity $\Delta\phi_{min}$ is found to be 2.3 dB below the SNL. For a larger number of photons in the interferometer, $\langle N(\Delta\lambda, \Delta\theta) \rangle = 11$, corresponding to $r_1 = 2.7$

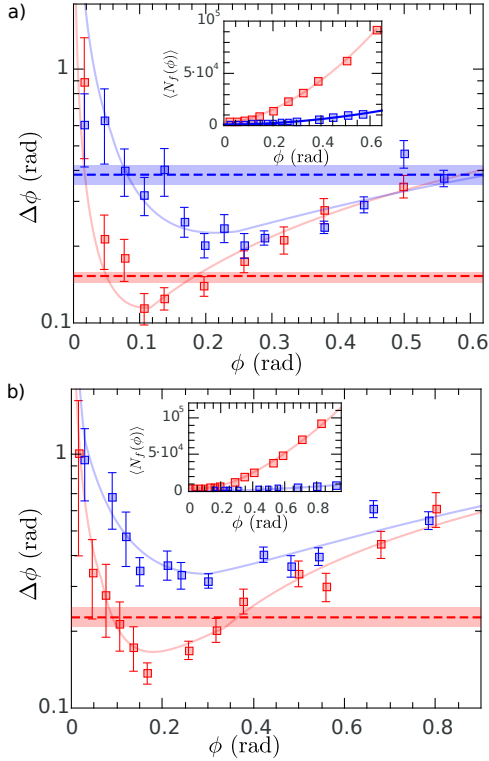


FIG. 3. Phase sensitivity measurements with $\Delta\theta = 0.9$ mrad and $\Delta\lambda = 3.1$ nm. a) Phase sensitivity for strongly differing gain values of BBO1: $r_1 = 1.5$, $\langle N(\Delta\lambda, \Delta\theta) \rangle = 1.7$ photons (blue), and $r_1 = 2.7$, $\langle N(\Delta\lambda, \Delta\theta) \rangle = 11$ photons (red). The values of $|r_2|$ are 4.9 and 5.2 respectively. The dashed lines mark the shot noise limited sensitivities $\Delta\phi_{SNL}$ for the two cases. b) Phase sensitivity for strongly differing gain values of BBO2: $|r_2| = 3.9$ (blue), $|r_2| = 5.2$ (red). The values of r_1 are 2.5 and 2.1 respectively. $\langle N(\Delta\lambda, \Delta\theta) \rangle = 4.8$ photons is the same in both cases and the corresponding $\Delta\phi_{SNL}$ is given by the dashed red line. The insets show the $\langle N_f(\phi) \rangle$ dependences.

and the gain of the second crystal almost the same, the SNL is overcome by 1.2 dB. The inset shows the corresponding $\langle N_f(\phi) \rangle$ dependences.

In Figure 3b, we show that a larger parametric gain of the second crystal leads to an improved sensitivity. Indeed, for $|r_2| = 3.9$ (blue curve), the best phase sensitivity is $\Delta\phi_{min} = 0.33$ rad while a larger parametric gain $|r_2| = 5.2$ obtained by increasing

the pump power gives $\Delta\phi_{min} = 0.16$ rad (red curve). The mean number of photons $\langle N(\Delta\lambda, \Delta\theta) \rangle = 4.8$ is kept constant by controlling the phase matching of BBO1. Hence the shot noise limit is the same in both cases and it is not beaten for the lower gain case.

Finally, we test the robustness of the scheme against the detection losses. For a given set $(r_1, |r_2|)$ of parametric gains, we vary the loss by adding neutral density filters before the detection. Figure 4 shows the measurement results for three sets of parametric gains. Theoretical dependencies taking into account the detector noise and the non-ideal visibility are also shown (see supplementary). The number of photons is kept constant, $N(\Delta\lambda, \Delta\theta) = 4.5 \pm 0.5$, for all three cases. The parametric gain of the second crystal is reduced from $|r_2| = 5.2$ (red points) to $|r_2| = 4.7$ (blue points) and $|r_2| = 4$ (green points). We can observe that for a large unbalancing of the interferometer, $|r_2|/r_1 = 2.5$ (red curve), the phase sensitivity is robust against the added losses, the system being still supersensitive for $\eta = 17\%$. For a smaller unbalancing of $|r_2|/r_1 = 1.9$ (blue curve), the sensitivity is degrading faster with the added losses. Finally, if the unbalancing is too weak $|r_2|/r_1 = 1.5$ (green curve), as was the case already in 3b, even without adding extra losses the interferometer cannot compensate for the detector noise and the sensitivity is therefore always above the SNL.

We would like to stress that this active detection strategy involving parametric amplification can also be implemented at the output of more common SU(2) interferometers (Mach-Zender, Michelson, Sagnac etc.). This is especially important in gravitational wave detectors where the detection losses considerably limit the sensitivity. Indeed, external elements of interferometers such as the Faraday isolators, output mode cleaners and photodetectors are reported as the main sources of losses [4]. Also the tolerance of the interferometer to detection losses is very important to experiments where a high phase sensitivity is required at frequency ranges (infrared, terahertz) where the efficiency of detectors is low for technical reasons. In addition, the unbalanced SU(1,1) interferometer can be reconfigured to be applied to sub-shot-noise imaging [25] where the detection efficiency plays a crucial role.

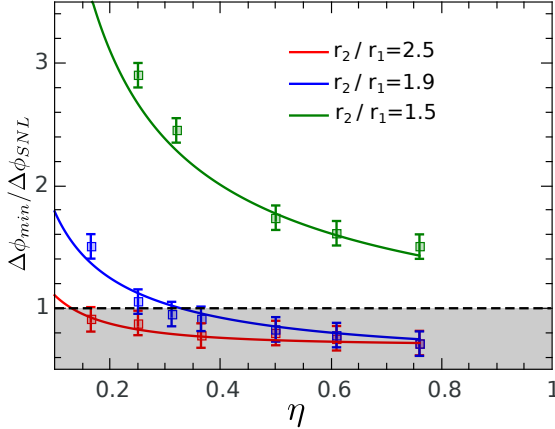


FIG. 4. Best phase sensitivity $\Delta\phi_{min}$ normalized to the shot noise limited sensitivity $\Delta\phi_{SNL}$ against the detection transmission η , reduced by adding neutral density filters. The number of photons is kept constant for all presented cases, with $\langle N(\Delta\lambda, \Delta\theta) \rangle = 4.5 \pm 0.5$. Red: $r_1 = 2.1$, $|r_2| = 5.2$. Blue: $r_1 = 2.5$, $|r_2| = 4.7$. Green: $r_1 = 2.6$, $|r_2| = 4$.

In conclusion, we have demonstrated for the first time phase supersensitivity in an unseeded SU(1,1) interferometer, beating the shot noise limit by 2.3 dB. Moreover we tested the robustness of this scheme against external losses. With the parametric gain 5.2, the SNL was beaten even for a detection efficiency as low as 17%. This result is very important for many cases where detection losses are high, such as gravitational-wave detection and phase measurements in the infrared and terahertz ranges.

We acknowledge the financial support of the joint DFG-RFBR project CH1591/2-1 - 16-52-12031 NNIOa

-
- [1] C. M. Caves, *Phys. Rev. D* **23**, 1693 (1981).
 - [2] M. Xiao, L.-A. Wu, and H. J. Kimble, *Physical review letters* **59**, 278 (1987).
 - [3] P. Grangier, R. Slusher, B. Yurke, and A. LaPorta, *Physical review letters* **59**, 2153 (1987).
 - [4] Abadie J. *et al*, *Nature Physics* **7**, 962 (2011).
 - [5] J. Aasi, J. Abadie, B. Abbott, R. Abbott, T. Abbott, M. Abernathy, C. Adams, T. Adams, P. Addesso, R. Adhikari, et al., *Nature Photonics* **7**, 613 (2013).
 - [6] M. Holland and K. Burnett, *Physical review letters* **71**, 1355 (1993).
 - [7] H. Lee, P. Kok, and J. P. Dowling, *Journal of Modern Optics* **49**, 2325 (2002).
 - [8] B. Yurke, S. L. McCall, and J. R. Klauder, *Phys. Rev. A* **33**, 4033 (1986).
 - [9] W. N. Plick, J. P. Dowling, and G. S. Agarwal, *New Journal of Physics* **12**, 083014 (2010).
 - [10] Z. Y. Ou, *Phys. Rev. A* **85**, 023815 (2012).
 - [11] A. Marino, N. C. Trejo, and P. Lett, *Physical Review A* **86**, 023844 (2012).
 - [12] C. Sparaciari, S. Olivares, and M. G. Paris, *Physical Review A* **93**, 023810 (2016).
 - [13] M. Manceau, F. Khalili, and M. Chekhova, *New Journal of Physics* **19**, 013014 (2017).
 - [14] J. Jing, C. Liu, Z. Zhou, Z. Y. Ou, and W. Zhang, *Applied Physics Letters* **99**, 011110 (2011), 10.1063/1.3606549.
 - [15] J. Kong, J. Jing, H. Wang, F. Hudelist, C. Liu, and W. Zhang, *Applied Physics Letters* **102**, 011130 (2013), 10.1063/1.4774380.
 - [16] F. Hudelist, J. Kong, C. Liu, J. Jing, Z. Ou, and W. Zhang, *Nature communications* **5** (2014).
 - [17] B. E. Anderson, P. Gupta, B. L. Schmittberger, T. Horrom, C. Hermann-Avigliano, K. M. Jones, and P. D. Lett, *arXiv preprint arXiv:1610.06891* (2016).
 - [18] D. Linnemann, H. Strobel, W. Muessel, J. Schulz, R. J. Lewis-Swan, K. V. Kheruntsyan, and M. K. Oberthaler, *Physical Review Letters* **117**, 013001 (2016).
 - [19] H. Hansen, T. Aichele, C. Hettich, P. Lodahl, A. Lvovsky, J. Mlynek, and S. Schiller, *Optics Letters* **26**, 1714 (2001).
 - [20] T. Iskhakov, M. V. Chekhova, and G. Leuchs, *Physical review letters* **102**, 183602 (2009).
 - [21] I. Agafonov, M. Chekhova, T. Iskhakov, and G. Leuchs, "Multimode detection of broadband squeezed vacuum."

- [22] A. M. Pérez, T. S. Iskhakov, P. Sharapova, S. Lemieux, O. V. Tikhonova, M. V. Chekhova, and G. Leuchs, *Opt. Lett.* **39**, 2403 (2014).
- [23] G. Rytikov and M. Chekhova, *Journal of Experimental and Theoretical Physics* **107**, 923 (2008).
- [24] A. Pérez, P. Sharapova, S. Straupe, F. Miatto, O. Tikhonova, G. Leuchs, and M. Chekhova, *Physical Review A* **92**, 053861 (2015).
- [25] G. Brida, M. Genovese, and I. Ruo Berchera, *Nature Photonics* **4**, 227 (2010).

Appendix A: Detection

The detectors are Hamamatsu S3883 p-i-n diodes with quantum efficiency 90% at 800 nm, followed by pulsed charge-sensitive amplifiers based on Amptek A250 and A275 chips, with peaking time 2.77 μ s. For each input light pulse, the output voltage pulse has a 8 μ s duration and the area depending on the input number of photons. The fundamental beam of the Spectra Physics Spitfire Ace system at $\lambda = 800$ nm is used to calibrate the detector. Figure 5a shows the mean area of the output voltage pulse for a given mean number of incoming photons per pulse. For each set of measurements presented in this work, the mean number of photons is derived from this calibration curve. One can see in Fig. 5a that the response of the detector to the light pulses is linear within most of the photon-number range under study in this work. However, as it is apparent in the inset of Fig. 5a for low photon fluxes ($\lesssim 2000$ photons per pulse), a nonlinearity, with a corresponding decrease in the detection sensitivity of the detector, needs to be taken into account.

Also, the detector brings some additional noise to the measurements. The corresponding noise in terms of photons per pulse is $\Delta N_d = 290$ photons in the linear part of the curve and considerably larger in its nonlinear part. The measurements presented in the main text are characterized by mean numbers of photons within a range of a few hundreds to a thousand in the region of interest for supersensitivity, *i.e.* around the dark fringe. A detector noise of $\Delta N_d \simeq 1000$ photons per pulse needs to be taken into account in this case.

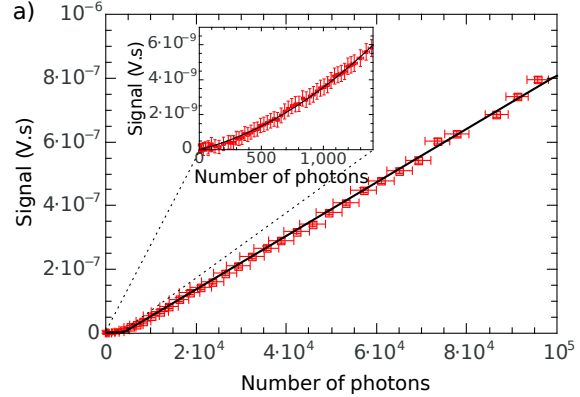


FIG. 5. a) Detector calibration curve, the mean area of the output voltage pulse versus the incoming mean number of photons per pulse. Above the level of 2000 photons per pulse, the detector shows a linear response. Inset: Zoom into the low-photon number part of the calibration curve showing a nonlinear behavior below 2000 photons per pulse.

Appendix B: Period of interferences and visibility

The interference period D is [22]

$$D = \frac{2\lambda_p}{\delta n_{air}}, \quad (\text{B1})$$

with λ_p the pump wavelength and $\delta n_{air} = n_{air}(400\text{nm}) - n_{air}(800\text{nm})$ the dispersion of the air gap between the two crystals for the considered pump and signal wavelengths. The laboratory temperature and humidity conditions give $D = 52$ mm. The phase ϕ can therefore be determined from D and the relative distance between the two crystals. A phase shift $\phi = \pi$ is equivalent to a 52 mm distance between the two crystals.

Figure 6 shows typical fringe patterns for two sets of parametric gain values. The distance between the crystals and the phase are arbitrarily set such that $\phi = 0$ corresponds to the dark fringe. A fit with Eq. (C5) gives a visibility $\mathcal{V} = 97\%$ in both cases, as well as for all the measurements reported in this article. The main reason for the visibility not exceeding 97% is that the interference is observed for spatially separated crystals. In this case, emission

from both of them is partially distinguishable and a 100% visibility can be achieved only by selecting a single plane wave, which would be the case for an infinitely small pinhole, $\Delta\theta = 0$.

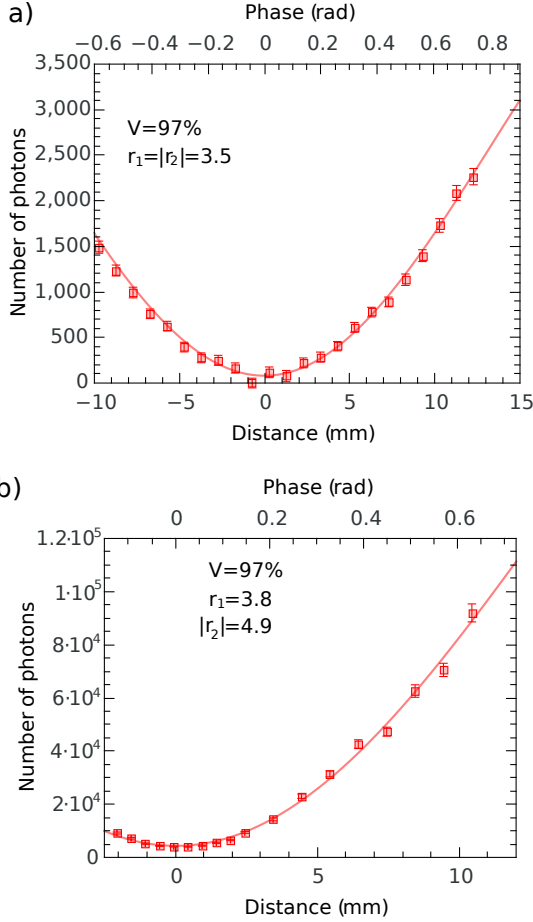


FIG. 6. Typical fringe patterns obtained for two sets of measurements characterized by different gain values. The fit is made with the expected $D = 52$ mm period from which the phase ϕ can be calculated.

Appendix C: Curve fitting, gain values

Following the calculations presented in Ref. [13], the interferometer output mean number of photons

$\langle N_f \rangle$ is given by

$$\langle N_f \rangle = \eta \nu [\mu |S(\phi)|^2 + (1 - \mu) \sinh^2 r_2], \quad (\text{C1})$$

with ν being the transmission of the squeezed mode through the spatial and frequency filters with bandwidth $\Delta\theta$, $\Delta\lambda$, η the detection efficiency of the setup for plane waves, μ the interferometer internal transmission and

$$S(\phi) = \sinh r_1 \cosh r_2 e^{-i\phi} - \cosh r_1 \sinh |r_2| e^{i\phi}. \quad (\text{C2})$$

As we work with high gain values, $\sinh r_1 \simeq \cosh r_1 \simeq \exp(r_1)/2$ and $\sinh r_2 \simeq \cosh r_2 \simeq \exp(r_2)/2$, which leads to a simplification of Eq. (C1),

$$\langle N_f \rangle \simeq \frac{1}{4} \eta \nu \mu \exp(2(r_1 + |r_2|)) \sin(\phi)^2 + \eta(1 - \mu) \exp(2|r_2|)/4. \quad (\text{C3})$$

Moreover, the mean number of photons inside the interferometer within the $\Delta\lambda$, $\Delta\theta$ bandwidths defined by the filters for the set of plane wave modes considered is

$$\langle N(\Delta\lambda, \Delta\theta) \rangle = \nu \sinh^2(r_1) \simeq \nu \exp(2r_1)/4. \quad (\text{C4})$$

Therefore,

$$\langle N_f \rangle \simeq \eta \mu \langle N(\Delta\lambda, \Delta\theta) \rangle \exp(2|r_2|) \sin(\phi)^2 + \eta(1 - \mu) \exp(2|r_2|)/4. \quad (\text{C5})$$

The number of photons in the interferometer $\langle N(\Delta\lambda, \Delta\theta) \rangle$ is measured with an avalanche photodiode and is therefore known. The internal transmission is also known, $\mu = 0.97$, as well as the detection efficiency $\eta = 0.77$. Thus the only unknown parameter in Eq. (C5) is $|r_2|$. The phase independent term $\eta(1 - \mu) \exp(2|r_2|)/4$ can be incorporated into a more general term, B , that also takes into account additional background light due to the non-perfect interference visibility:

$$\langle N_f \rangle \simeq \eta \mu \langle N(\Delta\lambda, \Delta\theta) \rangle \exp(2|r_2|) \sin(\phi)^2 + B. \quad (\text{C6})$$

The parametric gain of the first amplifier r_1 and the transmission ν of the squeezed mode can be subsequently found via Eq. (C4) and the number of

photons $\langle N_2(\Delta\lambda, \Delta\theta) \rangle$ produced by the second crystal in the $\Delta\theta, \Delta\lambda$ bandwidths, which is also measured:

$$\begin{aligned} r_1 &= \operatorname{asinh} \left(\sqrt{\frac{\langle N(\Delta\lambda, \Delta\theta) \rangle}{\langle N_2(\Delta\lambda, \Delta\theta) \rangle} \sinh^2 r_2} \right), \\ \nu &= \frac{\langle N(\Delta\lambda, \Delta\theta) \rangle}{\sinh^2(r_1)}. \end{aligned} \quad (\text{C7})$$

Figure 7 shows two examples of fit with Eq. (C6) for two datasets. The average pump power was set to 90 mW for the blue curve, while it was increased to 140 mW for the red curve. However the number of photons inside the interferometer $\langle N(\Delta\lambda, \Delta\theta) \rangle = 4.8$ is the same in both cases as the phase matching of the first crystal was modified in order to keep $\langle N(\Delta\lambda, \Delta\theta) \rangle$ constant for the two measurements. The second crystal is aligned such as to maximize the number of photons in the $\Delta\lambda, \Delta\theta$ windows. Hence the fits with Eq. (C6) yield $|r_2| = 3.9$ for the 90 mW pump power excitation, while the larger pump power of 140 mW gives a larger gain of $|r_2| = 5.2$. Furthermore we measured $\langle N_2(\Delta\lambda, \Delta\theta) \rangle$, the mean number of photons emitted by the second crystal within the bandwidths $\langle \Delta\lambda, \Delta\theta \rangle$. Using Eq. (C7), we find $r_1 = 2.5$ and $\nu = 0.13$ for the 90 mW case, while $r_1 = 2.1$ and $\nu = 0.29$ for the 140 mW case. It is to be noted that different transmission ν of the squeezed mode are found for the two measurements because the mode size changes while changing the phase matching of the first crystal.

Appendix D: post-processing

The pump beam possesses a relatively good intensity stability with a pulse energy fluctuation around 10 nJ for the mean pulse energy of 20 μJ .

The corresponding second-order correlation function at zero delay is $g^{(2)}(0) = \frac{\langle I^2 \rangle}{\langle I \rangle^2} \approx 1.00001$, with I being the measured pump beam intensity. The pump intensity distribution is therefore almost Poissonian ($g^{(2)}(0) \approx 1$). However because of the high parametric gains involved in the measurements, these small-scale pump intensity fluctuations are amplified in the PDC light. We use an additional BBO crystal $\chi_{pp}^{(2)}$ to enhance these fluctuations and be in the sensitive wavelengths range of the p-i-n diode used. The broadband, multimode PDC light generated by $\chi_{pp}^{(2)}$ is then measured by a second p-i-n diode PD2 similar to PD1. A post-processing window is set to discard from a measurement set excitation pulses falling out a high and a low signal threshold. Hence, the pump fluctuations are decreased and the mean number of photons for a given interferometer position can be measured precisely.

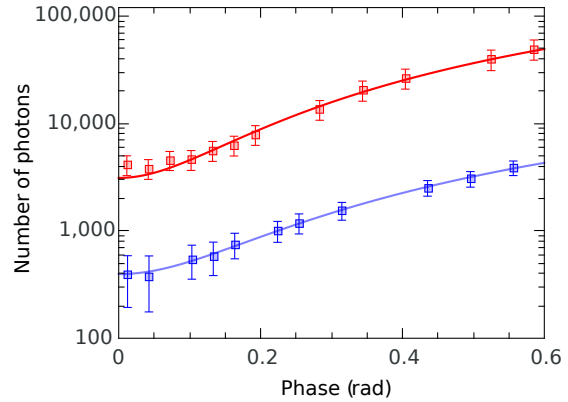


FIG. 7. Example of two sets of data fitted by Eq. (C5). Red curve: pump power 140 mW, $|r_2| = 5.2$, $r_1 = 2.1$ and $\nu = 0.29$. Blue curve: pump power 90 mW, $|r_2| = 3.9$, $r_1 = 2.5$ and $\nu = 0.13$.